catalysts

MDPI

Article

Mango Seed-Derived Hybrid Composites and Sodium Alginate Beads for the Efficient Uptake of 2,4,6-Trichlorophenol from Simulated Wastewater

Asma Jabeen [1], Urooj Kamran [2,3], Saima Noreen [1], Soo-Jin Park [2,*] and Haq Nawaz Bhatti [1,*]

[1] Department of Chemistry, University of Agriculture, Faisalabad 38000, Pakistan
[2] Department of Chemistry, Inha University, 100 Inharo, Incheon 22212, Korea
[3] Department of Mechanical Engineering, College of Engineering, Kyung Hee University, Yongin 445-701, Korea
* Correspondence: sjpark@inha.ac.kr (S.-J.P.); hnbhatti2005@yahoo.com (H.N.B.); Tel./Fax: +92-333-6528455 (H.N.B.)

Abstract: In this study, mango seed shell (MS)-based hybrid composite and composite beads ($FeCl_3$-$NaBH_4$/MS and Na-Alginate/MS) were designed. Batch and column experimental analyses were performed for the uptake of 2,4,6-trichlorophenol (2,4,6-TCP) from wastewater. The physicochemical characteristics of both composites were also examined. From the batch adsorption experiments, the best adsorption capacities of 28.77 mg/g and 27.42 mg/g were observed in basic media (pH 9–10) at 308 K for $FeCl_3$-$NaBH_4$/MS and 333 K for Na-Alginate/MS with 25 mg/L of 2,4,6-TCP concentration for 120 min. The rate of reaction was satisfactorily followed by the pseudo-second-order kinetics. Equilibrium models revealed that the mechanism of reaction followed the Langmuir isotherm. The thermodynamic study also indicated that the nature of the reaction was exothermic and spontaneous with both adsorbents. Desorption experiments were also carried out to investigate the reliability and reusability of the composites. Furthermore, the efficiency of the adsorbents was checked in the presence of different electrolytes and heavy metals. From the batch experimental study, the $FeCl_3$-$NaBH_4$/MS composite proved to be the best adsorbent for the removal of the 2,4,6-TCP pollutant, hence it is further selected for fixed-bed column experimentation. The column study data were analyzed using the BDST and Thomas models and the as-selected $FeCl_3$-$NaBH_4$/MS hybrid composites showed satisfactory results for the fixed-bed adsorption of the 2,4,6-TPC contaminants.

Keywords: mango seed shell; hybrid composite; alginate; 2,4,6-trichlorophenol; adsorption

Citation: Jabeen, A.; Kamran, U.; Noreen, S.; Park, S.-J.; Bhatti, H.N. Mango Seed-Derived Hybrid Composites and Sodium Alginate Beads for the Efficient Uptake of 2,4,6-Trichlorophenol from Simulated Wastewater. *Catalysts* **2022**, *12*, 972. https://doi.org/10.3390/catal12090972

Academic Editor: Sagadevan Suresh

Received: 25 July 2022
Accepted: 25 August 2022
Published: 30 August 2022

1. Introduction

Contamination by volatile phenolic compounds threatens the use of water resources. Phenolic compounds with an unpleasant odor and a half-life span of 2–72 days cause extremely toxic effects in water [1–3]. Phenolic compounds are widely used in various products such as pharmaceuticals, plastics manufacturing, petrochemicals, oil refineries, pesticide/insecticide units, leather, paper, paint, wood, and other chemical manufacturing processes [4,5]. The wastewater discharged from the manufacture of these products contains many toxic phenolic compounds which are considered important to treat before discharge into water reservoirs [6]. Due to the toxicity of these phenolic pollutants, the U.S. Environmental protection agency lists the most phenolic pollutants as hazardous to human health and other living organisms [7,8]. Therefore, the discharge or removal of these hazardous pollutants is highly significant. The World Health Organization (W.H.O.) recommends the permissible concentration of phenolics to be about 0.001 mg/L in potable water and less than 1 mg/L in industrial wastewater for the safe discharge of polluted water into the environment [9,10].

Until now, various methods have been used for the elimination of phenolic contaminants from wastewater including biological, chemical, and electrochemical treatments

and adsorption, photochemical oxidation, and catalytic reduction [11–13]. Among these, adsorption is considered the most convenient, eco-friendly, and cost-effective technique for the treatment of wastewater [14,15]. Adsorption is also trending due to its ease of operation, flexibility and lowest production of harmful by-products [16,17]. Various adsorbing materials or catalysts have been employed for the treatment of wastewater to eliminate various phenolic pollutants and other contaminants such as metal oxides, minerals, zeolites, polymers, activated carbons, and carbon nanotubes [18–21]. The use of polymers and biopolymers as adsorbents has become a well-established purification method, providing good efficiency to eliminate various toxic pollutants from water in a short time [22,23]. Biomass-based polymeric materials, such as rice husks, sugarcane bagasse, cotton sticks, coconut shells, leaves and barks of different plats, waste teas, seeds of plants, and seed shells of different fruits, provide a highly polymeric and porous structure that favors the adsorption mechanism [24–28].

Recently, the use of activated carbon, magnetically active materials, nanomaterials, chemically modified composites, and hybrid materials has gained more attention from researchers due to their modified structures and extensive adsorption properties [29–31]. The chemical and polymeric blending and grafting of materials are trending due to their excellent performance in wastewater treatment [32]. The synthesis of composites and modification of polymeric materials have also been used to resolve the disposal issue of waste slug, which is mostly produced during the treatment of water with simple or native biomasses as adsorbents [33–36].

Hence, this work is focused on the fabrication of an $FeCl_3$-$NaBH_4$-modified mango seed shell (MS)-based hybrid composite ($FeCl_3$-$NaBH_4$/MS) and sodium alginate-modified mango seed shell (MS)-based composite beads (Na-Alginate/MS) for the adsorptive removal of 2,4,6-trichlorophenol from aqueous media. The adsorption properties and structural changes on the surface of the polymeric structure of the adsorbents were determined by FTIR, TGA, and SEM analytical techniques. The experimental work was performed in batch and column modes for the optimization of various parameters. The reusability and recovery of adsorbents after adsorption experiments is also a concerning process for researchers; therefore, desorption experiments were also performed to check the reusability and percentage of recovery of both adsorbents ($FeCl_3$-$NaBH_4$/MS and Na-Alginate/MS) after experimentation.

2. Results and Discussion

2.1. Functional, Thermal, and Morphological Analysis of Composite Materials

FTIR spectra for both adsorbents ($FeCl_3$-$NaBH_4$/MS and Na-Alginate/MS) before and after adsorption for the comparative study are given in Figure 1a,b. The examination of the different functional groups shows that there were a different number of groups present such as a broad peak observed at 1030 cm^{-1} associated with C-O stretching vibration in primary and secondary alcohols some other peaks observed at 1575–1735 cm^{-1} mostly for the aromatic bending of the C=C groups associated with the aromatic ring, and some medium-intensity peaks observed at 1420 cm^{-1}, indicating the presence of O-H bending associated with phenol [37–39]. Similarly, a strong and broad peak was observed at 3330 cm^{-1} for the O-H stretching in the aromatic ring [40,41]. Some bands' intensities were found to be decreased after the adsorption spectra, indicating the decline in the number of functional groups after the adsorption of the 2,4,6-TCP contaminants.

Thermo-gravimetric analyses were performed to determine the thermal stability of both composites at an increasing temperature rate of 10 °C/min. As illustrated in Figure 1c,d, the decompositions of the composites' structures due to the elimination of volatile compounds occurred at high temperatures. A very small reduction in weight was observed at the initial 150 min of the temperature stage due to the removal of the loosely bound moisture content from the surface of the composites. The Na-Alginate/MS composite beads have a high moisture content compared to the $FeCl_3$-$NaBH_4$/MS hybrid composite and it experiences a consistent decrease in weight loss from the start of the

reaction. The initial stages of weight loss were observed due to the elimination of the lignin and hemicellulose functional groups from the structure of the composites after 230 °C [42]. Another prominent stage of weight loss of about 80% was observed in the case of $FeCl_3$-$NaBH_4$/MS just after 350–400 °C due to the elimination of aromatic derivatives from the base structure (Figure 1c) [43], but in the case of the Na-Alginate/MS composite beads, only a 60% weight loss was observed at this point and the composition of Na-Alginate/MS showed better structural stability up to 560 °C (Figure 1d). In addition, a >80% weight loss was found after 400 °C in the case of $FeCl_3$-$NaBH_4$/MS and about an 80% weight loss was observed after 600 °C in the case of Na-Alginate/MS. However, the remaining backbone structure with 20% weight remained stable even after 800 °C.

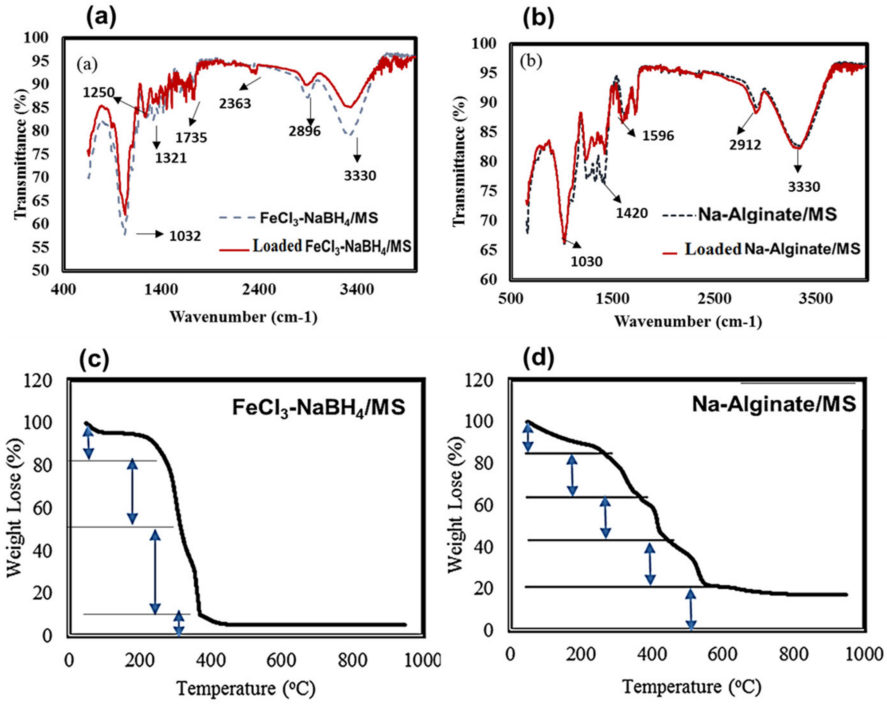

Figure 1. FTIR spectra of (**a**) $FeCl_3$-$NaBH_4$/MS hybrid composites and (**b**) Na-Alginate/MS composite beads, both for loaded and unloaded 2,4,6-TCP, and TGA thermograms for (**c**) $FeCl_3$-$NaBH_4$/MS hybrid composites and (**d**) Na-Alginate/MS composite beads.

The surface morphological structural characteristics were determined by SEM-EDX analysis for both adsorbents ($FeCl_3$-$NaBH_4$/MS and Na-Alginate/MS). Figure 2a,b present the rough and porous structure of the adsorbents that facilitates the adsorption of pollutant molecules. The rough and porous surface of the adsorbents is related to their efficiency in the uptake of pollutants and the porous surface is usually capable of enhancing adsorption capacity [30]. In addition, the presence of different functional groups on the surface (as determined by FTIR) also played an important role in the adsorption performance of the 2,4,6-TCP molecules on the surface of the adsorbents.

2.2. Batch Experimental Study

2.2.1. Influence of pH

In the batch adsorption study, the pH is considered an important factor that influences the capacity of the adsorbent [44,45]. The current study was carried out to check the efficiency of adsorbents in acidic and basic media. To determine the dependency of the adsorption reaction on the pH, the reactions were performed at a pH range of 2–10 with both adsorbents. It was observed from the q_e values that were obtained at the end of each experiment, that the adsorption capacities of 2,4,6-TCP were more favorable in the basic media. As 2,4,6-TCP was founded as a neutral molecule at pH 6.15, the anionic form of 2,4,6-TCP on the increasing pH influenced by the electrostatic force between the negatively

charged TCP anion and the adsorbent molecules ($FeCl_3$-$NaBH_4$/MS and Na-Alginate/MS composites) results in an increase in adsorption capacity up to pH 10 (Figure 3a). Further increases in the pH cause the aggregation of pollutant molecules that affects the capacities of the adsorbents [46,47]. Olu-Owolabi and coworkers carried out the adsorption of 2,4,6-T on KAC and PCK and found an increase in adsorption capacity with increasing adsorbent doses up to pH 9 [48]. The variability of the pH was found to be high for PCK compared to KAC at a pH between 6 and 10. This could be due to the increase in electrostatic attraction between 2,4,6-T and KAC in this pH region, which enhanced the adsorption capacity, although the PCK showed less adsorption efficiency in the acidic pH region due to the limited functional groups on the surface.

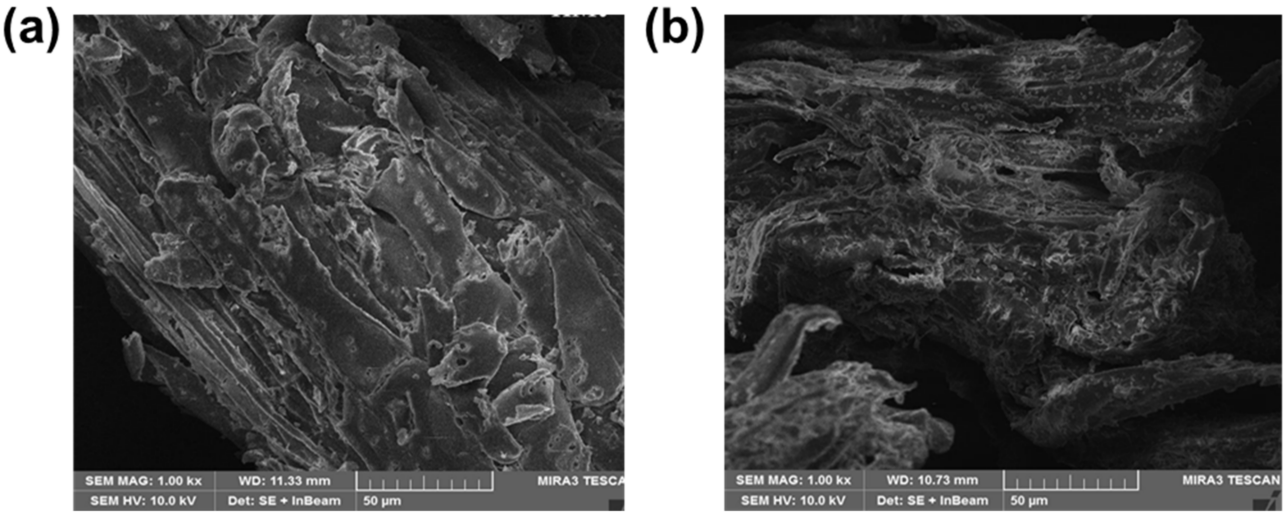

Figure 2. SEM micrographs of (**a**) $FeCl_3$-$NaBH_4$/MS hybrid composites and (**b**) Na-Alginate/MS composite beads.

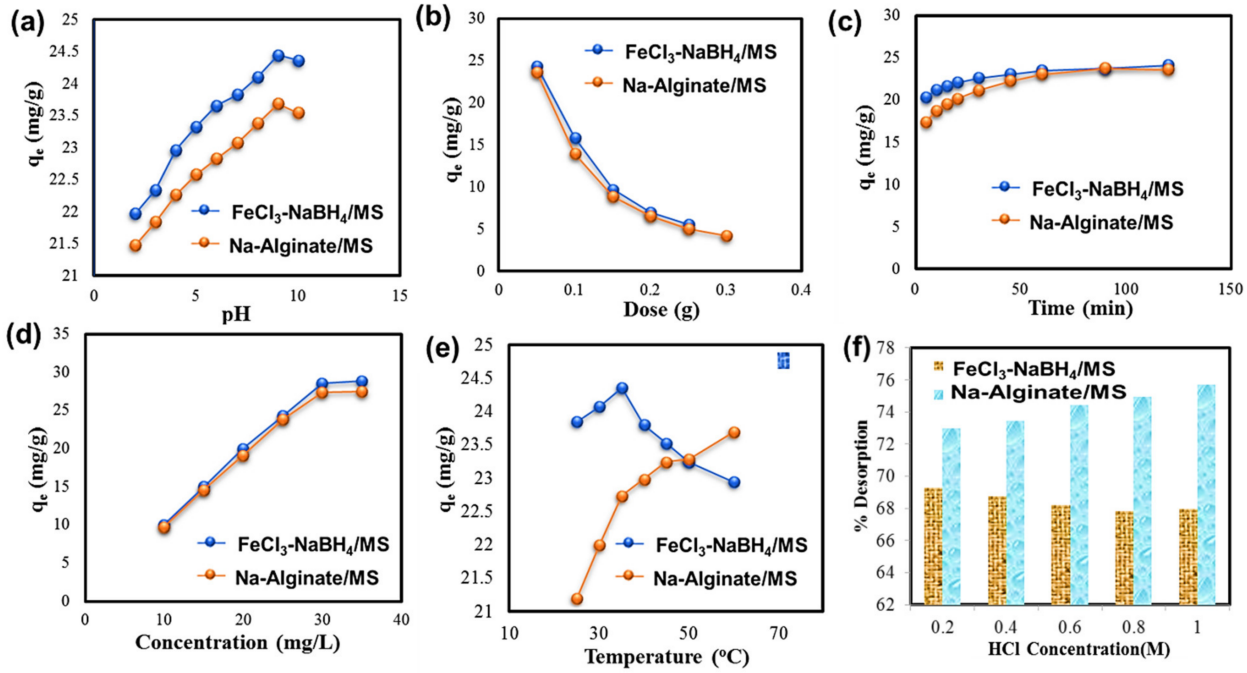

Figure 3. Influence of (**a**) pH, (**b**) dose, (**c**) contact time, (**d**) 2,4,6-TCP initial concentration, and (**e**) temperature on 2,4,6-TCP adsorption capacities of adsorbents and (**f**) 2,4,6-TCP contaminant desorption efficiency of adsorbents in desorbing agents.

2.2.2. Influence of Adsorbent Dosage

The increase in the adsorbent dose provides the opportunity for the pollutants to attach to the maximum available active sites of the adsorbent. The effect of increasing the adsorbent dose for the adsorption of 2,4,6-TCP onto $FeCl_3$-$NaBH_4$/MS and Na-Alginate/MS composites was determined in this study. It was found that by increasing the amount of the adsorbent from 0.1 to 0.4 g, the adsorption capacities were decreased as shown in Figure 3b. As there were a high number of active sites for the adsorption of the pollutant molecules for the available concentration of the 2,4,6-TCP molecules, these molecules occupied all available sites and on further increasing the dose [49,50], the number of active sites increased but as the concentration was fixed, this led to decreased q_e values [51]. A similar phenomenon was observed previously [52] for phenolic compounds, where a decrease in sorption capacity (q_e) with increasing adsorbent doses was considered a reason for the unsaturation of active binding sites in an adsorption phenomenon. The same trend was also reported by El-Naas and coworkers for the adsorption of phenol onto date-pit activated carbon [53]. They found that the phenol concentration decreased with the increasing adsorbent dose, which provided more adsorption sites for phenol and increased the adsorption rate. However, at a specific level, the available active sites were more than the available phenol molecules, which resulted in a decline in adsorption capacity.

2.2.3. Influence of Contact Time and Kinetic Study

The rate of the adsorption reaction between the adsorbents and 2,4,6-TCP molecules was investigated under various time intervals. The adsorption capacity of 2,4,6-TCP at a concentration of 25 mg/L with 0.05 mg of composites was determined. As shown in Figure 3c, at the start of the reaction for both adsorbents, a rapid increase in the rate of adsorption was observed (in the first 30–60 min of reaction) because all of the surface sites became occupied by the available pollutant molecules; after saturation of the active sites (up to 60 min), the adsorption process slowed down due to the hindrance of the occupying pollutant molecules and stopped at a point where maximum adsorption occurred [54–56]. The adsorption kinetic models, pseudo-first-order and pseudo-second-order, and the intraparticle model of diffusion were applied to predict the adsorption of the 2,4,6-TCP contaminants onto the $FeCl_3$-$NaBH_4$/MS and Na-Alginate/MS composites. Linear plots of ln ($q_e - q_t$) vs time were obtained to determine the rate constant [8]. The linear equation (Equation (2)) derived from Equation (1) can be used to calculate the constant values for the pseudo-first-order reaction

$$\frac{d_q}{d_t} = k_1(q_e - q_t) \tag{1}$$

$$\log(q_e - q_t) = \log q_e - \frac{k_1}{2.303}t \tag{2}$$

In the above equations, k_1 (min^{-1}) is the first-order rate constant, q_e and q_t (mg/g) are the equilibrium adsorption capacities for 2,4,6-TCP, and t (min) is the adsorption time [57]. Similarly, the differential and linear form of pseudo-second-order reactions can be written as Equations (3) and (4):

$$\frac{d_t}{q_t} = k_2(q_e - q_t)^2 \tag{3}$$

$$\frac{t}{q_t} = \frac{1}{k_2 q_e^2} + \frac{t}{q_t} \tag{4}$$

In the above equations, q_e and q_t (mg/g) are the adsorption capacities at the equilibrium and time (t), whereas, k_2 is used to represent the rate constant of the pseudo-second-order reaction.

The intraparticle diffusion model was used to determine the diffusion of the phenolic molecules into the inner pores of the adsorbents. This model shows the interaction of molecules towards the binding adsorption sites and influences the biosorption efficiency

of adsorbents [58]. The equation used to calculate the values of the intraparticle diffusion constants is given below:

$$q_t = k_{pi} t^{1/2} + C_i \quad (5)$$

The values for the kinetic rate constants (k) and correlation coefficients (R^2) are given in Table 1 and the kinetic linear plots are illustrated in Figure 4a–c. If the values of R^2 were found close to unity ($\geq$0.999), they showed the best fitness of the respective kinetic models. In the current study, the R^2 values of the pseudo-second-order reactions found as the maximum (0.999 for both adsorbents), as well as the closeness of calculated and experimental q_e values also showing the best fitness of the pseudo-second-order kinetic model (Table 1).

Table 1. Kinetic constant parameters for the adsorption of 2,4,6-TCP onto $FeCl_3$-$NaBH_4$/MS and Na-Alginate/MS composites.

Kinetic Model	$FeCl_3$-$NaBH_4$/MS	Na-Alginate/MS
Pseudo 1st order		
q_e exp. (mg/g)	24.11	23.75
q_e cal. (mg/g)	−0.363	−0.091
K_1 (min^{-1})	0.014	0.028
R^2	0.632	0.922
Pseudo 2nd order		
q_e exp. (mg/g)	24.11	23.75
q_e cal. (mg/g)	24.39	24.93
K_2 (g mg^{-1} min^{-1})	0.022	0.012
R^2	0.999	0.999
Intraparticle diffusion		
K_{pi}	0.411	0.735
R^2	0.923	0.920
C_i	19.99	16.64

2.2.4. Influence of Initial Concentration and Equilibrium Studies

The number of pollutants highly influenced the adsorption capacities of the adsorbents. In order to investigate this influence, various concentrations (10, 15, 20, 25, 30, and 35 mg/L) of 2,4,6-TCP were investigated at fixed amounts of adsorbents (0.05 g). As shown in Figure 3d, it was found that with the increasing concentration of the pollutant, the adsorption capacities increased up to the saturation of all adsorption sites and this saturation was achieved at a 30 mg/L concentration of 2,4,6-TCP. The mechanism followed by the adsorption reaction was determined by applying various theoretical equilibrium models such as Langmuir, Freundlich, Temkin, Harkins-Jura (H-J), and Doubinin-Radushkevich (D-R) to the experimental data. The optimized contact time that allowed us to study the mechanism of the reaction was 120 min for each experiment.

The linear form of the Langmuir isotherm was used, which is based on the formation of a monolayer between the finite number of adsorbate-adsorbent identical sites having a homogeneous distribution of energy overall binding sites [59]. Equation (6) presents the linear form of the Langmuir isotherm:

$$\frac{C_e}{q_e} = \frac{1}{q_m b} + \frac{C_e}{q_m} \quad (6)$$

where q_m and q_e (mg/g) are the maximum and equilibrium adsorption capacities, respectively, and b (L/mg) and C_e (mg/L) are the binding energies and equilibrium concentrations. The Freundlich isotherm provided the idea for the heterogeneity of surface binding sites

and favored the multilayer adsorption mechanism [60]. The linear form presented in Equation (7) was used to calculate the values of the Freundlich parameters:

$$\log q_e = \log k_F + \frac{1}{n} \log C_e \tag{7}$$

In the above equation, k_F is the Freundlich constant, and q_e (mg/g) and C_e (mg/g) are the adsorption capacities and concentrations at equilibrium. Another equilibrium isothermal model named Temkin expresses homogeneous energy distribution on the active sites and heat of the adsorption [61]. Equation (8) presents the linear form of the Temkin isotherm:

$$q_e = B \ln A + B \ln C_e \tag{8}$$

Both A and B are Temkin's constants. A plot between q_e and lnC_e (equilibrium adsorption capacities and concentrations) was drawn to calculate the values of the Temkin's constants (A and B). Another equilibrium model the H-J isotherm based on the multilayer adsorption phenomena on the heterogeneous distribution of energy sites was also used [62]. The linear form of this model is given in Equation (9) and was used to calculate the values of the H-J constants (A and B):

$$\frac{1}{q_e^2} = \left(\frac{B}{A}\right) - \left(\frac{1}{A}\right) \log C_e \tag{9}$$

The D-R model rejected the idea of the Langmuir model (homogeneous energy distribution) and used a linear equation to estimate the apparent free-energy binding sites on the adsorbent surfaces [63]. The linear form of the D-R model as given in Equations (10) and (11) helps to calculate the biosorption energy (β) and Polanyi potential (ε) of the D-R isotherm:

$$\ln q_e = \ln q_m - \beta \varepsilon^2 \tag{10}$$

$$\varepsilon = RT \ln\left(1 + \frac{1}{C_e}\right) \tag{11}$$

In Equation (11), R is the general gas constant (8.314 J·mol^{-1}K^{-1}) and T (K) is the absolute temperature. Similarly, the value of mean free energy (E) can be calculated by Equation (12):

$$E = \frac{1}{\sqrt{2\beta}} \tag{12}$$

The Elovich model explains the multilayer adsorption phenomenon of the pollutants on the exponentially increasing active binding sites on the surface of the adsorbents. The linear form of the Elovich model [64,65] is presented in Equation (13):

$$\ln \frac{q_e}{C_e} = \ln K_E q_{\max} - \frac{q_e}{q_{\max}} \tag{13}$$

where, K_E presents the Elovich constant (L/mg), C_e is the equilibrium 2,4,6-TCP concentration, and q_m shows the maximum calculated adsorption capacity (mg/g) from the Elovich isotherm. The values of K_E, q_{max}, and the regression coefficient R^2 were calculated by plotting a graph, ln (q_e/C_e) vs. q_e (Table 2).

The calculated and experimental values for all isotherms along with their correlation values are given in Table 2. By comparing the regression values of all isothermal models, we determined the fitness of the best model in order to find the mechanism that was being followed by the batch experiment at various concentrations of pollutants. The R^2 values of the Langmuir model showed the best fitness of this model on the experimental data with very high R^2 values (0.999 and 0.996) for both adsorbents ($FeCl_3$-$NaBH_4$/MS and Na-Alginate/MS) compared to the other isothermal models. Furthermore, the fitness of the Langmuir model can be verified by comparing the calculated and experimental q_e values.

In addition, the D-R model also showed good fitness with a high R^2 value (0.945) for only the $FeCl_3$-$NaBH_4$/MS hybrid composite.

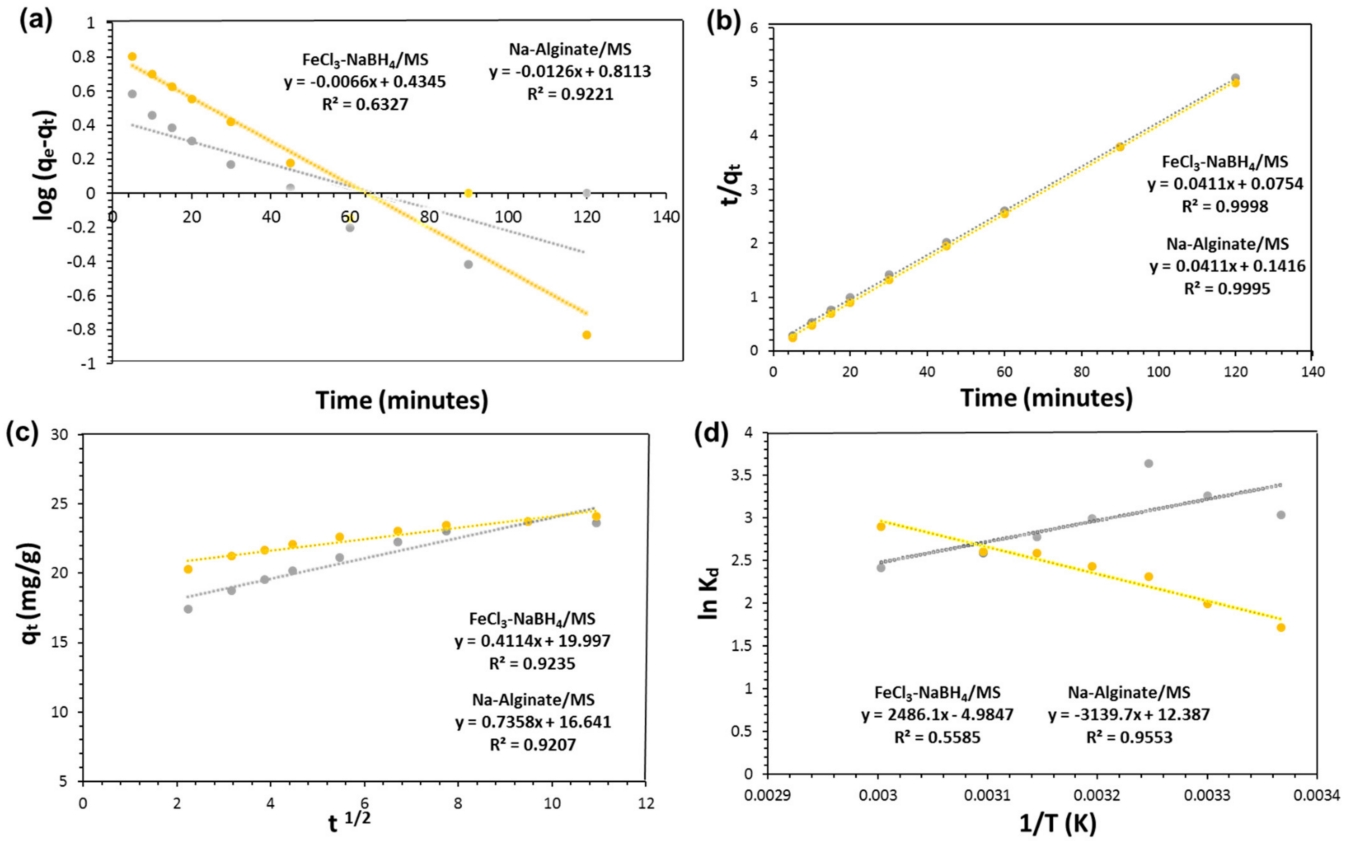

Figure 4. Kinetic plots for 2,4,6-TCP adsorption (**a**) Pseudo 1st order, (**b**) Pseudo 2nd order, (**c**) Intraparticle diffusion, and (**d**) adsorption thermodynamics of 2,4,6-TCP above $FeCl_3$-$NaBH_4$/MS and Na-Alginate/MS composites.

2.2.5. Influence of Temperature and Thermodynamics Studies

To determine the effect of increasing temperature on the uptake of 2,4,6-TCP onto the $FeCl_3$-$NaBH_4$/MS and Na-Alginate/MS composites, experiments were performed at different temperatures ranging from 297 to 333 K. It was found that the adsorption capacities of the $FeCl_3$-$NaBH_4$/MS hybrid composite decreased after 308 K, but increased for the Na-Alginate/MS composite bead up to 323 K, showing the stability of the active sites for the adsorption of 2,4,6-TCP molecules at this temperature (Figure 3e). The values for the various thermodynamic parameters (enthalpy "ΔH", entropy "ΔS", and Gibbs free energy "ΔG") were calculated to determine the nature of the chemical reaction that occurred on the surface of the adsorbents [66] using Equations (14)–(16):

$$\Delta G^\circ = \Delta H^\circ - T\Delta S^\circ \quad (14)$$

$$\Delta G^\circ = -RT \ln K_d \quad (15)$$

In the above equation, R is a gas constant (8.314 J·mol^{-1}K^{-1}), T (K) is the temperature, and K_d is a thermodynamics constant. The value of K_d can be determined using Equation (16):

$$\ln(K_d) = \frac{\Delta S^\circ}{R} - \frac{\Delta H^\circ}{R} \times \frac{1}{T} \quad (16)$$

As shown in Table 3, in the case of the 2,4,6-TCP adsorption performance on the Na-Alginate/MS composite beads, the decreasing values of ΔG on increasing temperatures up to 333 K were noticed due to the spontaneous nature of the reaction. The positive values

of ΔH show the endothermic nature of the reaction as the heat evolved and the entropy (ΔS) of the system increased [37,40]. On the other hand, in the case of the $FeCl_3$-$NaBH_4$/MS hybrid composite, the adsorption only favorable at temperature up to 308 K, hence the values of ΔG first decreased then increased after 308 K (Figure 4d). The value of ΔH was negative, showing the exothermic nature of the reaction; as the heat contents decreased the value of ΔS also decreased compared to the value observed in the case of adsorption with the Na-Alginate/MS composite beads.

Table 2. Equilibrium isothermal constant parameters of 2,4,6-TCP onto $FeCl_3$-$NaBH_4$/MS and Na-Alginate/MS composites.

Isothermal Models	*Composites*	
Langmuir	**$FeCl_3$-$NaBH_4$/MS**	**Na-Alginate/MS**
K_L	0.998	0.013
b	0.0005	2.119
q_{max} Cal. (mg/g)	28.99	29.49
q_{max} Exp. (mg/g)	28.77	27.42
R^2	0.999	0.996
Freundlich		
K_F (mg/g)	0.144	0.096
n	7.018	3.114
R^2	0.771	0.786
D-R		
q_m (mg/g)	8.1×10^{11}	4.2×10^{11}
β 10^4(mol^2/kL^2)	0.00001	0.0001
E	235.71	70.71
R^2	0.863	0.945
Temkin		
A	9.284	3.23
B	2.73	5.85
R^2	0.852	0.848
Harkins–Jura		
A	0.001	0.109
B	0.267	0.226
R^2	0.503	0.775
Elovich		
K_E (L/mg)	12.838	1.4898
q_{max} Cal. (mg/g)	3.911	11.299
q_{max} Exp. (mg/g)	28.77	27.42
R^2	0.784	0.647

Table 3. Thermodynamic parameters for the adsorption of 2,4,6-TCP onto $FeCl_3$-$NaBH_4$/MS and Na-Alginate/MS composites.

	$FeCl_3$-$NaBH_4$/MS			**Na-Alginate/MS**		
Temp. (K)	**$\Delta G°$ (kJ·mol^{-1})**	**$\Delta H°$ (kJ·mol^{-1})**	**$\Delta S°$ (kJ/mol·K)**	**$\Delta G°$ (kJ·mol^{-1})**	**$\Delta H°$ (kJ·mol^{-1})**	**$\Delta S°$ (kJ/mol·K)**
297	−7.49			−4.24		
303	−8.20			−5.01		
308	−9.31			−5.91		
313	−7.77	−20.74	0.042	−6.33	26.19	0.103
318	−7.33			−6.83		
323	−6.94			−6.997		
333	−6.68			−8.01		

2.3. Desorption Study

Desorption is an important parameter to check the efficiency of adsorbents for a number of repeated cycles [67]. This study was carried out in the presence of different molar concentrations (0.2, 0.4, 0.6, 0.8, and 1 M) of HCl solutions. The percentage of pollutant desorbed was calculated using the percent desorption formula in Equation (17):

$$Desorption\% = \frac{\text{Amount of pollutant desorbed } \left(\frac{\text{mg}}{\text{g}}\right)}{\text{Amount of pollutant sorbed}} \times 100 \quad (17)$$

For the desorption analysis of the 2,4,6-TCP pollutants, the molar solutions of HCl were used for both adsorbents because the best adsorption capacities in batch experiments were observed in basic media. From Figure 3f, it was found that on increasing the HCl concentration up to 1 M, the 2,4,6-TCP desorption capacities were increased [16,24] and up to 75% of Na-Alginate/MS and 69% of $FeCl_3$-$NaBH_4$/MS were successfully recovered.

2.4. Influence of Electrolytes and Heavy Metals

The effect of different electrolytes and heavy metals on the adsorption capacity of both adsorbents was investigated. In these experiments, the effects of different electrolytes, such as Na^+, K^+, Al^{3+}, Mg^{2+}, and Ca^{2+}, and heavy metals, such as Cr Cu, Co, Pb, and Cd, at fixed 2,4,6-TCP concentrations (25 mg/L) were examined. The amounts of adsorbents were also kept optimum (0.05 g) and the reactions were performed at ambient temperatures for 120 min. It was observed that the presence of electrolytes Ca^{2+} and Al^{3+} slightly fluctuated the adsorption capacities of both adsorbents compared to the control values (Figure 5a). Similarly, the presence of heavy metals caused a prominent decrease in the adsorption capacities with the $FeCl_3$-$NaBH_4$/MS hybrid composite but a slight reduction with the Na-Alginate/MS composite beads as shown in Figure 5b. This small fluctuation was due to the aggregation of metal ions in the solution phase that resisted the attachment of the pollutant molecules on the surface of the adsorbents but was enhanced in the presence of electrolytes [30,37].

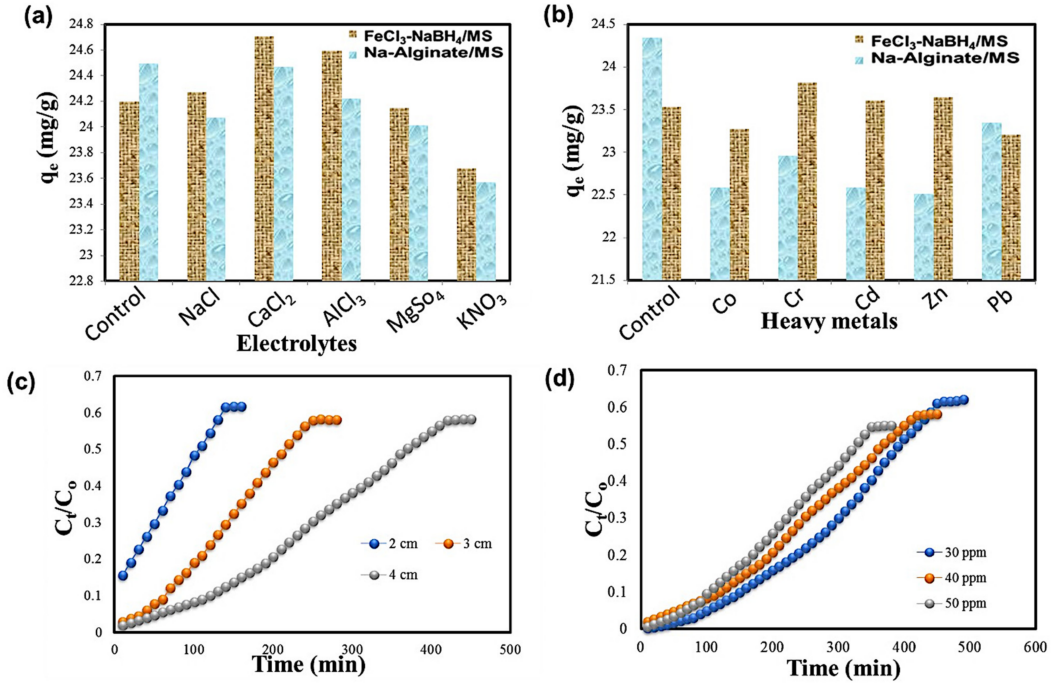

Figure 5. (**a**) Effect of different electrolytes, (**b**) effect of various heavy metals towards adsorption performance of 2,4,6-TCP onto $FeCl_3$-$NaBH_4$/MS and Na-Alginate/MS composites, and (**c**,**d**) effect of bed height on the uptake of 2,4,6-TCP by the $FeCl_3$-$NaBH_4$/MS hybrid composite.

2.5. Column Study

The efficiency of the selected adsorbent ($FeCl_3$-$NaBH_4$/MS) based on the best adsorption power was also investigated in column study experiments. The effects of different process parameters, such as bed height and pollutant concentration, were investigated at a fixed flow rate of 1.8 mL/min. The salient feature of continued study experimentation is its breakthrough time, which helps to investigate the effectiveness of the adsorbent's bed height and the renaissance time of the column [68]. The breakthrough time (Q_{50}) was calculated by Equation (18) using the values of breakthrough time (BT), flow rate, the concentration of 2,4,6-TCP (C_i), and the mass of the $FeCl_3$-$NaBH_4$/MS hybrid composite in the column bed:

$$\text{BT capacity}(Q_{50\%}) = \frac{\text{BT time(at 50\%)} \times \text{flowrate} \times C_i}{\text{Mass of adsorbent in bed(g)}} \quad (18)$$

The calculated values of breakthrough time and capacities are given in Table 4 along with bed height concentrations and flow rates.

Table 4. Breakthrough point and capacities at various conditions for 2,4,6-TCP uptake by $FeCl_3$-$NaBH_4$/MS hybrid composite.

Inlet Conc. (ppm)	Bed Height (cm)	Flow Rate ($mL \cdot min^{-1}$)	Breakthrough Point (50%) (min)	Biosorption Capacity (mg/g)
30	4	1.8	400	14.4
40	2	1.8	100	14.4
40	3	1.8	210	15.12
40	4	1.8	360	17.28
50	4	1.8	300	18

2.5.1. Influence of Bed Height

The effect of the column study parameter bed height was determined using different amounts of the $FeCl_3$-$NaBH_4$/MS adsorbent at a fixed-inlet 2,4,6-TCP concentration (40 mg/L) with a fixed flow rate (1.8 mL/min). As seen in Figure 5c, the adsorption capacity of $FeCl_3$-$NaBH_4$/MS increased on increasing the bed height from 2 to 4cm; the maximum recorded adsorption capacity of $FeCl_3$-$NaBH_4$/MS was 17.28 mg/g at 360 min. It was also found that the shifting of the breakthrough time toward higher values was due to the availability of an increased number of vacant sites with the increasing bed height of the column [45,69]. This increasing number of active sites favored the uptake of more pollutant (2,4,6-TCP) molecules by intra-particulate diffusion. A higher breakthrough time means a longer stay for the pollutants in the column and as a result, more effluent was being treated. The calculated values of the breakthrough time are given in Table 4.

2.5.2. Influence of 2,4,6-TCP Initial Dye Concentration

The effect of another parameter pollutant of the 2,4,6-TCP concentrations was also investigated in the column study experiments. Measurements of different concentrations of 30, 40, and 50 mg/L of 2,4,6-TCP were taken by keeping the bed height and flow rate constant, at 3 cm and 1.8 mL/L, respectively (Figure 5d). It was concluded that on the increasing concentration of 2,4,6-TCP, the adsorption capacity was also increased from 14.4 mg/g (with 30 mg/L) to 18 mg/g (with 50 mg/L of pollutant concentration). The decrease in the breakthrough time was noticed due to the presence of a high concentration gradient at an increased concentration of 2,4,6-TCP as it increased the rate of the reaction [70,71]. The available active sites saturated faster with the available concentration of 2,4,6-TCP as this concentration was enough to saturate the active sites by reducing the breakthrough time. This effect steepened the curve by reducing the BT volume due to the availability of weak driving forces for the mass transfer from the bulk to the surfaces of the adsorbents [72].

2.5.3. Models for Column Study

Two kinetic models including the Thomas and BDST (bed-depth service time) models were applied to the experimental data in the column study of the two parameters in order to investigate the performance of the adsorbent in the column.

The Thomas model is based on the concept of the Langmuir isotherm and second-order reversible kinetics at equilibrium followed by the driving force present between the pollutants and adsorbent molecules. The second-order kinetics (reversible) and Langmuir isotherm can be used under favorable or unfavorable conditions [73]. The linear form of the Thomas model used for the calculations of different constants is given in Equation (19),

$$\ln\left(\frac{C_o}{C_t} - 1\right) = \frac{K_{Th} \times q_o \times W}{Q} - K_{Th} \times C_o \times t \quad (19)$$

In the above equation, K_{Th} (mL/min.mg) is a rate constant of the Thomas model, the C_o (mg/L) for the inlet and C_t (mg/L) for the outlet are the 2,4,6-TCP concentrations, q_o (mg/g) is for the 2,4,6-TCP uptake at equilibrium, W (g) is the mass of the $FeCl_3$-$NaBH_4$/MS adsorbent, t (min) is the time and Q (mL/min) is the flow rate. The calculated values of the parameters are presented in Table 5. The higher calculated values of R^2 and close values of the adsorption capacities (observed values with the calculated values) showed the fitness of the Thomas model on the experimental data. It was also observed that with increasing concentrations, the rate of the inter-phase mass transfer decreased [48,74].

Table 5. Thomas model parameters for the adsorption of 2,4,6-TCP onto $FeCl_3$-$NaBH_4$/MS hybrid composite.

Inlet Conc. (mg/L)	Bed Height (cm)	Flow Rate (mL/min)	K_{Th} (mL/min) × 10^3	q_e cal. (mg/g)	q_e exp. (mg/g)	R^2
30	4	1.8	0.00037	14.27	14.4	0.924
40	2	1.8	0.00035	14.85	14.4	0.980
40	3	1.8	0.00035	15.95	15.12	0.954
40	4	1.8	0.00025	17.14	17.28	0.982
50	4	1.8	0.00024	18.92	18	0.917

The BDST model was used to investigate the relationship between the amount of adsorbent in the bed (bed-depth Z) and the adsorbent efficiency (service time t) and was applied to the experimental values obtained from the column experimental studies (effect of initial 2,4,6-TCP concentration and bed height). The service time in this model can be defined as "this is the maximum time at which adsorbent remains able to remove pollutant from solution before regeneration is required" or "the time taken by the column bed to attain the breakthrough point" [19,75,76]. The calculations of the different parameters of this model were carried out using the linear form given in Equation (20):

$$t = \frac{N_o Z}{C_o U} - \frac{1}{K_a C_o} \ln\left(\frac{C_o}{C_b} - 1\right) \quad (20)$$

In the above equation, C_o and C_b (mg/L) are the initial and BT (breakthrough) concentrations of 2,4,6-TCP, U is the linear velocity, K_a is the rate constant of the BDST model, N_o and Z (cm) are the biosorption capacity and bed height, respectively [71]. The values of the parameters for the BDST model were calculated using the values of the slope and intercept of the graph and are presented in Table 6.

$$t = aZ \quad (21)$$

where,

$$Slope = a = \frac{N_o}{C_o U} \quad (22)$$

Table 6. BDST model parameters for the adsorption of 2,4,6-TCP onto $FeCl_3$-$NaBH_4$/MS hybrid composite.

C_t/C_o	A	B	K_a (L·mg^{-1}·min^{-1}) × 10^4	N_o (mg·L^{-1}) × 10^{-4}	R^2
0.2	85	−151.6	0.00024	1938	0.998
0.4	100	−110	0.00012	2280	0.970
0.6	145	−168.3	0.00004	3306	0.990

And

$$Intercept = b = \frac{1}{K_a C_o} \ln\left(\frac{C_o}{C_b} - 1\right) \quad (23)$$

The values of R^2 obtained at different bed heights illustrate the fitness of the BDST model on the experimental data of the column study.

3. Synthetic Methodologies

3.1. Chemical Reagents and Biomass

Phenolic pollutants named 2,4,6-trichlorophenol (2,4,6-TCP) were supplied by AGROSOL Ltd., Karachi, Pakista. All reagents and chemicals sodium borohydride ($NaBH_4$), iron(III) chloride hexahydrate ($FeCl_3 \cdot 6H_2O$), ethanol, sodium alginate, polyvinyl alcohol (PVA), calcium chloride ($CaCl_2$), boric acid, NaCl solution (saline), NaOH, and HCl used throughout the experiments were of analytical grade and purchased from Sigma-Aldrich (Saint Louis, MO, USA). The mango seed shell biomass was purchased from the local market in the city of Faisalabad, Pakistan.

3.2. Preparation of Composite and Composite Beads

Mango seed shell (MS) biomass-based $FeCl_3$-$NaBH_4$/MS hybrid composite and Na-Alginate/MS composite beads were prepared following the reported methodology [54,77]. In order to prepare $FeCl_3$-$NaBH_4$/MS hybrid composites, first, 2 g of washed and ground MS biomass (particle size 300 µm) was soaked in 0.1 M of HCl solution (200 mL) for 1 h and 30 min. Then, the MS biomass was washed several times with deionized water and oven dried at 60 °C. The dried MS biomass was added to a 0.05 M $FeCl_3.6H_2O$ solution at a 1:1 ratio and stirred at 250 rpm on a magnetic stirrer. Then, 10 mL of 0.53 M ($NaBH_4$) was poured into the mixture and it was further stirred at 150 rpm. Products (precipitates) were filtered, washed with ethanol, and dried in an oven at 50 °C overnight.

Similarly, the MS biomass-based sodium alginate composite beads (Na-Alginate/MS) were synthesized by preparing a solution of PVA (3.5 g) and sodium alginate (1 g) in deionized water. This solution was stirred at 50 °C for 30 min, and then 1.5 g of biomass was added and it was further stirred for 1 h under the same experimental conditions. Then, 0.1 M of $CaCl_2$ (500 mL) and boric acid were prepared. The mixture of biomass-PVA and Na-Alginate was poured drop-wise into this solution for the formation of the Na-Alginate/MS composite beads. The as-prepared composite beads were separated from the solution after 24 h, washed with saline solution several times, and stored in saline solution at 5 °C.

3.3. Characterization of Composites

FTIR Cary-630 (Fourier transform infrared spectrometer) (Agilent Technologies, Clara, CA 95051, USA) was used to determine the functional group modifications that occurred on the surface of the MS biomass after the formation of the composites; spectra were recorded in the IR region 4000–500 cm^{-1} before and after the adsorption. The surface textures and morphological properties of the adsorbents were determined by a JMT-300 SEM-EDS (scanning electron microscopy paired with energy dispersive X-ray) (JEOL Ltd. Akishima, Tokyo, Japan). Surface information was obtained at 1.0 kx–25.0 kx magnifications and 11 mm focus distances. Similarly, a TGA/DSA Axxx multi-analyzer (Metter Toledo, Columbus, OH, USA) was used to analyze the thermal stability of the composites. Approximately 40–70 mg

(300 µm size) samples were taken into the sampler and heated at a temperature range of 10–900 °C with an increasing temperature rate of 10 °C/min under a nitrogen atmosphere.

3.4. Preparation of 2,4,6-TCP Stock Solution

A stock solution of 2,4,6-TCP was prepared by dissolving 1 g per 1000 mL of deionized water. Further diluted solutions of low concentrations of 10–25 mg/L (25 ppm) were prepared from this stock solution for the batch experiments.

3.5. Experimental Batch Study

Batch experimental work was performed to check the effect of the different batch-adsorption parameters on the adsorption behavior of both adsorbents ($FeCl_3$-$NaBH_4$/MS and Na-Alginate/MS). The effect of the pH was examined at a pH range of 2–9; contact time experiments were performed at different time intervals such as 5, 10, 15, 20, 30, 45, 60, 90, and 120 min; the effects of the pollutant concentrations were checked at a range of 2,4,6-TCP initial concentrations of 10, 25, 30, 40, and 50 mg/L; and the temperature effect experiment was carried out at room temperature (about 297 K), 303, 308, 313, 318, 323, and 333 K. Similarly, the effect of different adsorbent doses of 0.05, 0.1, 0.15, 0.2, 0.25, and 0.3 g were investigated for both adsorbents. Other effects such as the presence of different electrolytes and heavy metals were also examined in the batch study experiments. Different studies were carried out for the adsorption of the phenolic compounds in the batch experiments. The adsorption capacity values of some reported adsorbents [55,78–80] for the adsorption of the phenolic compounds are given in Table 7. The process diagram for the batch adsorption reaction is presented in Figure 6a.

Table 7. Comparison of adsorption capacities reported in current work and adsorption capacities of other adsorbents reported by various researchers.

Pollutants	Adsorbent	Initial Concentration (mg/L)	Adsorption Capacity (mg/g)	Reference
2,6-dichlorophenol	Modified plantain peel adsorbents	50–100	15.9	[54]
Para-Chlorophenol	Magnetic powdered activated carbon	100–150	66.5	[78]
2,4,6-Trichlorophenol	Modified polypropylene hollow fiber composites	40–100	66.49	[79]
2,4,6-Trichlorophenol	chitosan/fly-ash-based magnetic composites	100–150	68.89	[80]
Bisphenol A	chitosan/fly-ash-based magnetic composites	50–150	31.92	[80]
2,4,6-Trichlorophenol	Fe^{3+}- and Fe^{2+}-enriched magnetic composites	35–50	31.27	[55]
2,4,6-Trichlorophenol	$FeCl_3$-$NaBH_4$/MS	10–35	28.77	This Study
2,4,6-Trichlorophenol	Na-Alginate/MS	10–35	27.42	This Study

3.6. Desorption Study

The efficiency of the adsorbents depends on the reliability and reusability of the adsorbents at different cycles. The percentage of desorption of the adsorbents after the adsorption experiments is directly related to the efficiency of the adsorbents. Desorption experiments were performed using different HCl molar concentrations (as desorbing agents) for the recovery of the composites.

3.7. Column Study

The column study was carried out in a glass column with a diameter of 1.2 cm and a path length of 42 cm. The effects of the different column study parameters, such as bed height and the concentration of 2,4,6-TCP, were investigated at a fixed flow rate of 1.8 mL/min. The inlet pollutant concentrations (30, 40, and 50 mg/L) and bed heights (1.5, 2.5, and 3.5 g) of the adsorbents at 1, 2, and 3 cm column lengths were investigated

with the $FeCl_3$-$NaBH_4$/MS hybrid composites. A bit of glass wool was used to hold the adsorbent inside the column. All the experiments were carried out at room temperature and with a solution at pH 9, which was obtained from the batch study experiments. The outlet concentrations after adsorption were analyzed at 10 min intervals of time by a Uv-Vis spectrophotometer to calculate the C_i/C_o ratios. The process diagram for the fixed-bed column experiments is given in Figure 6b.

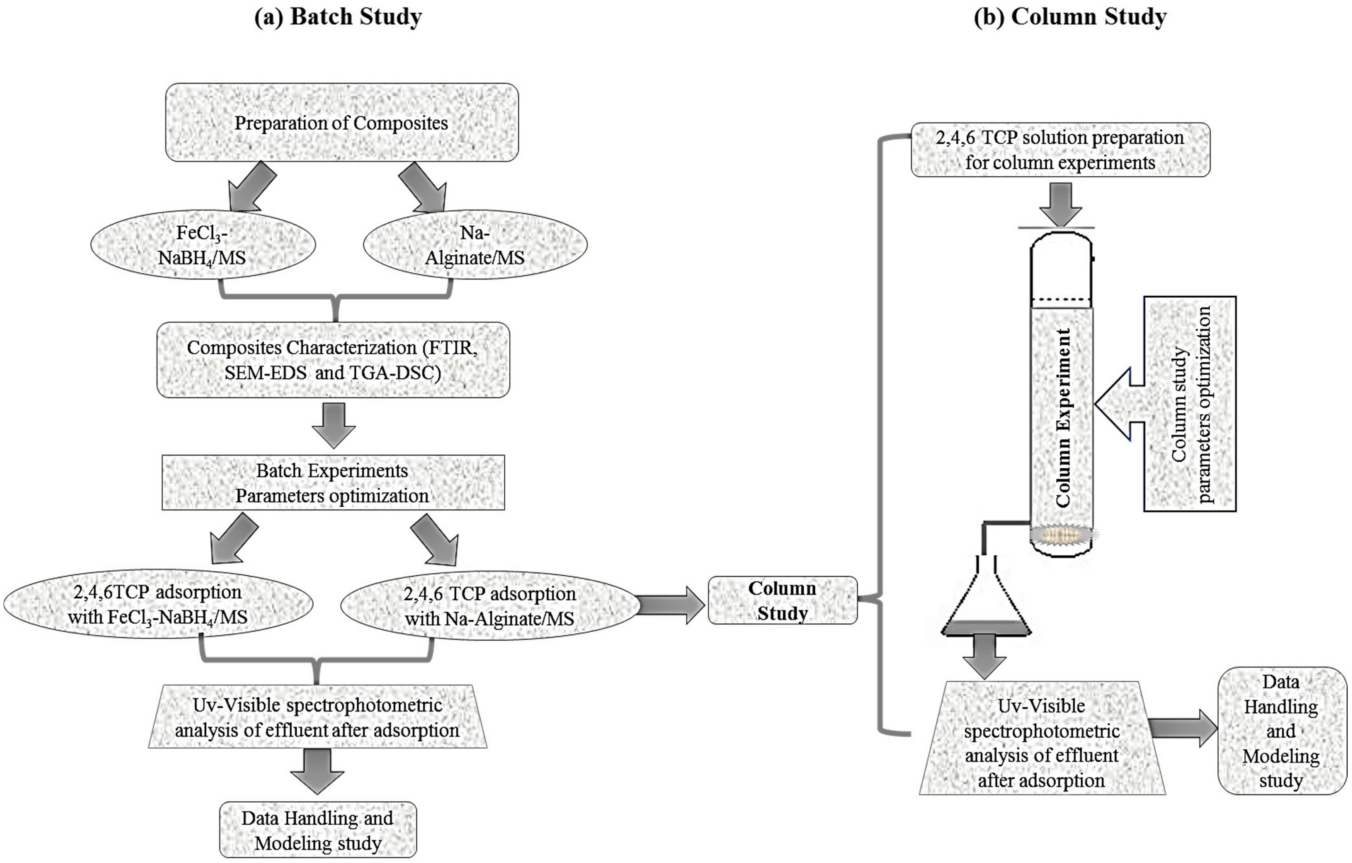

Figure 6. Flow sheet diagram for (**a**) Batch study experiments and (**b**) column study experiments.

4. Conclusions

In summary, mango seed shell biomass-based hybrid composite and composite beads ($FeCl_3$-$NaBH_4$/MS and Na-Alginate/MS) were successfully investigated for the removal of 2,4,6-TCP pollutants from wastewater. Both composites were considered efficient and low-cost adsorption materials for the removal of phenolics from wastewater. The batch experiments illustrate that the best working adsorption conditions were pH: alkaline 9–10, dose: 0.05 g, adsorption equilibrium time: 120 min at temperatures of 308 K (for $FeCl_3$-$NaBH_4$/MS) and 333 K (for Na-Alginate/MS), and 2,4,6-TCP initial concentration: 25 mg/L. The results obtained in the batch experiments were also tested by applying kinetics, equilibrium, and thermodynamic models and the best-fitting models were the pseudo-second-order and Langmuir for both the kinetics and equilibrium data. The thermodynamic models showed the exothermic, endothermic, and spontaneous or non-spontaneous nature of the chemical reactions. The best-working adsorbent ($FeCl_3$-$NaBH_4$/MS) was selected for column study experiments and investigated by applying the column study parameters, bed height, and increasing initial concentration parameters. The experimental data were also best fitted with the column study models (Thomas and BDST) with high R^2 values. From the results, it can be concluded that the as-designed $FeCl_3$-$NaBH_4$/MS hybrid composite and Na-Alginate/MS composite beads can be considered efficient adsorbents for the adsorptive removal of 2,4,6-TCP or other phenolic compounds from wastewater at the commercial level.

Author Contributions: Conceptualization, A.J.; investigation, A.J.; writing—original draft preparation, A.J.; writing—review, A.J.; writing—review & editing, U.K. and S.N.; Help and Support in data handling, S.-J.P.; supervision, H.N.B.; All authors have read and agreed to the published version of the manuscript.

Funding: This work did not receive any external funding and this research work was conducted in the Department of Chemistry, University of Agriculture, Faisalabad, Pakistan; and this work was also supported by Department of Chemistry, Inha University, Incheon, South Korea, and the Department of Mechanical Engineering, Kyung Hee University, Yongin, South Korea These institutes provided all the facilities to conduct this research and modeling work.

Data Availability Statement: Not applicable.

Acknowledgments: The authors are thankful to the Department of Chemistry, University of Agriculture, Faisalabad, Pakistan for providing some of the research facilities. In addition to this, the authors are also thankful to the Polymer-Carbon Nanomaterials Laboratory, the Department of Chemistry, Inha University, Incheon, South Korea, and the Department of Mechanical Engineering, Kyung Hee University, Yongin, South Korea, for providing some of the instrumental analytical facilities and the modeling for this work.

Conflicts of Interest: The authors declare no conflict of interest.

References

1. Devi, P.; Saroha, A.K. Simultaneous adsorption and dechlorination of pentachlorophenol from effluent by Ni–ZVI magnetic biochar composites synthesized from paper mill sludge. *Chem. Eng. J.* **2015**, *271*, 195–203. [CrossRef]
2. Wang, L.; Gan, K.; Lu, D.; Zhang, J. Hydrophilic Fe_3O_4 @C for High-Capacity Adsorption of 2,4-Dichlorophenol. *Eur. J. Inorg. Chem.* **2016**, *2016*, 890–896. [CrossRef]
3. Shi, W.; Ren, H.; Huang, X.; Li, M.; Tang, Y.; Guo, F. Low cost red mud modified graphitic carbon nitride for the removal of organic pollutants in wastewater by the synergistic effect of adsorption and photocatalysis. *Sep. Purif. Technol.* **2019**, *237*, 116477. [CrossRef]
4. Pei, Z.; Li, L.; Sun, L.; Zhang, S.; Shan, X.-Q.; Yang, S.; Wen, B. Adsorption characteristics of 1,2,4-trichlorobenzene, 2,4,6-trichlorophenol, 2-naphthol and naphthalene on graphene and graphene oxide. *Carbon* **2013**, *51*, 156–163. [CrossRef]
5. Liu, H.; Ruan, X.; Zhao, D.; Fan, X.; Feng, T. Enhanced Adsorption of 2,4-Dichlorophenol by Nanoscale Zero-Valent Iron Loaded on Bentonite and Modified with a Cationic Surfactant. *Ind. Eng. Chem. Res.* **2016**, *56*, 191–197. [CrossRef]
6. Hasan, Z.; Jhung, S.H. Removal of hazardous organics from water using metal-organic frameworks (MOFs): Plausible mechanisms for selective adsorptions. *J. Hazard. Mater.* **2015**, *283*, 329–339. [CrossRef]
7. Heo, J.; Yoon, Y.; Lee, G.; Kim, Y.; Han, J.; Park, C.M. Enhanced adsorption of bisphenol A and sulfamethoxazole by a novel magnetic CuZnFe2O4–biochar composite. *Bioresour. Technol.* **2019**, *281*, 179–187. [CrossRef]
8. Ahmad, N.; Al-Fatesh, A.S.; Wahab, R.; Alam, M.; Fakeeha, A.H. Synthesis of silver nanoparticles decorated on reduced graphene oxide nanosheets and their electrochemical sensing towards hazardous 4-nitrophenol. *J. Mater. Sci. Mater. Electron.* **2020**, *31*, 11927–11937. [CrossRef]
9. Kwon, J.; Lee, B. Bisphenol A adsorption using reduced graphene oxide prepared by physical and chemical reduction methods. *Chem. Eng. Res. Des.* **2015**, *104*, 519–529. [CrossRef]
10. Jin, M.-Y.; Lin, Y.; Liao, Y.; Tan, C.-H.; Wang, R. Development of highly-efficient ZIF-8@PDMS/PVDF nanofibrous composite membrane for phenol removal in aqueous-aqueous membrane extractive process. *J. Membr. Sci.* **2018**, *568*, 121–133. [CrossRef]
11. Chen, X.H.; Shan, Z.J.; Zhai, H.L. QSAR models for predicting the toxicity of halogenated phenols to *Tetrahymena*. *Toxicol. Environ. Chem.* **2016**, *99*, 273–284. [CrossRef]
12. Gomri, M.; Abderrazak, H.; Chabbah, T.; Souissi, R.; Saint-Martin, P.; Casabianca, H.; Chatti, S.; Mercier, R.; Errachid, A.; Hammami, M.; et al. Adsorption characteristics of aromatic pollutants and their halogenated derivatives on bio-based poly (ether-pyridine)s. *J. Environ. Chem. Eng.* **2020**, *8*, 104333. [CrossRef]
13. Pham, T.D.; Bui, T.T.; Truong, T.T.T.; Hoang, T.H.; Le, T.S.; Duong, V.D.; Yamaguchi, A.; Kobayashi, M.; Adachi, Y. Adsorption characteristics of beta-lactam cefixime onto nanosilica fabricated from rice HUSK with surface modification by polyelectrolyte. *J. Mol. Liq.* **2019**, *298*, 111981. [CrossRef]
14. Kamran, U.; Park, S.-J. Microwave-assisted acid functionalized carbon nanofibers decorated with Mn doped TNTs nanocomposites: Efficient contenders for lithium adsorption and recovery from aqueous media. *J. Ind. Eng. Chem.* **2020**, *92*, 263–277. [CrossRef]
15. Kamran, U.; Park, S.-J. Functionalized titanate nanotubes for efficient lithium adsorption and recovery from aqueous media. *J. Solid State Chem.* **2019**, *283*, 121157. [CrossRef]
16. Shankar, A.; Kongot, M.; Saini, V.K.; Kumar, A. Removal of pentachlorophenol pesticide from aqueous solutions using modified chitosan. *Arab. J. Chem.* **2020**, *13*, 1821–1830. [CrossRef]
17. Naganathan, K.K.; Faizal, A.N.M.; Zaini, M.A.A.; Ali, A. Adsorptive removal of Bisphenol a from aqueous solution using activated carbon from coffee residue. *Mater. Today: Proc.* **2021**, *47*, 1307–1312. [CrossRef]

18. Zhu, H.; Li, Z.; Yang, J. A novel composite hydrogel for adsorption and photocatalytic degradation of bisphenol A by visible light irradiation. *Chem. Eng. J.* **2018**, *334*, 1679–1690. [CrossRef]
19. Batra, S.; Datta, D.; Beesabathuni, N.S.; Kanjolia, N.; Saha, S. Adsorption of Bisphenol-A from aqueous solution using amberlite XAD-7 impregnated with aliquat 336: Batch, column, and design studies. *Process Saf. Environ. Prot.* **2018**, *122*, 232–246. [CrossRef]
20. Men, X.; Guo, Q.; Meng, B.; Ren, S.; Shen, B. Adsorption of bisphenol A in aqueous solution by composite bentonite with organic moity. *Microporous Mesoporous Mater.* **2020**, *308*, 110450. [CrossRef]
21. Kamran, U.; Heo, Y.-J.; Lee, J.W.; Park, S.-J. Chemically modified activated carbon decorated with MnO_2 nanocomposites for improving lithium adsorption and recovery from aqueous media. *J. Alloy. Compd.* **2019**, *794*, 425–434. [CrossRef]
22. Duan, F.; Chen, C.; Zhao, X.; Yang, Y.; Liu, X.; Qin, Y. Water-compatible surface molecularly imprinted polymers with synergy of bi-functional monomers for enhanced selective adsorption of bisphenol A from aqueous solution. *Environ. Sci. Nano* **2016**, *3*, 213–222. [CrossRef]
23. Enyoh, C.E.; Isiuku, B.O. 2,4,6-Trichlorophenol (TCP) removal from aqueous solution using Canna indica L.: Kinetic, isotherm and Thermodynamic studies. *Chem. Ecol.* **2020**, *37*, 64–82. [CrossRef]
24. Sahnoun, S.; Boutahala, M.; Zaghouane-Boudiaf, H.; Zerroual, L. Trichlorophenol removal from aqueous solutions by modified halloysite: Kinetic and equilibrium studies. *DESALINATION Water Treat.* **2015**, *57*, 15941–15951. [CrossRef]
25. Obinna, I.B.; Ebere, E.C. A review: Water pollution by heavy metal and organic pollutants: Brief review of sources, effects and progress on remediation with aquatic plants. *Anal. Methods Environ. Chem. J.* **2019**, *2*, 5–38. [CrossRef]
26. Kamran, U.; Park, S.-J. MnO_2-decorated biochar composites of coconut shell and rice husk: An efficient lithium ions adsorption-desorption performance in aqueous media. *Chemosphere* **2020**, *260*, 127500. [CrossRef]
27. Kamran, U.; Bhatti, H.N.; Noreen, S.; Tahir, M.A.; Park, S.-J. Chemically modified sugarcane bagasse-based biocomposites for efficient removal of acid red 1 dye: Kinetics, isotherms, thermodynamics, and desorption studies. *Chemosphere* **2021**, *291*, 132796. [CrossRef]
28. Kamran, U.; Bhatti, H.N.; Iqbal, M.; Jamil, S.; Zahid, M. Biogenic synthesis, characterization and investigation of photocatalytic and antimicrobial activity of manganese nanoparticles synthesized from Cinnamomum verum bark extract. *J. Mol. Struct.* **2018**, *1179*, 532–539. [CrossRef]
29. Tan, I.A.W.; Ahmad, A.L.; Hameed, B.H. Adsorption isotherms, kinetics, thermodynamics and desorption studies of 2,4,6-trichlorophenol on oil palm empty fruit bunch-based activated carbon. *J. Hazard. Mater.* **2009**, *164*, 473–482. [CrossRef]
30. Mubarik, S.; Saeed, A.; Athar, M.; Iqbal, M. Characterization and mechanism of the adsorptive removal of 2,4,6-trichlorophenol by biochar prepared from sugarcane baggase. *J. Ind. Eng. Chem.* **2016**, *33*, 115–121. [CrossRef]
31. Lisowski, P.; Colmenares, J.C.; Mašek, O.; Lisowski, W.; Lisovytskiy, D.; Kamińska, A.; Łomot, D. Dual Functionality of TiO_2/Biochar Hybrid Materials: Photocatalytic Phenol Degradation in the Liquid Phase and Selective Oxidation of Methanol in the Gas Phase. *ACS Sustain. Chem. Eng.* **2017**, *5*, 6274–6287. [CrossRef]
32. Gundogdu, A.; Duran, C.; Senturk, H.B.; Soylak, M.; Ozdes, D.; Serencam, H.; Imamoglu, M. Adsorption of Phenol from Aqueous Solution on a Low-Cost Activated Carbon Produced from Tea Industry Waste: Equilibrium, Kinetic, and Thermodynamic Study. *J. Chem. Eng. Data* **2012**, *57*, 2733–2743. [CrossRef]
33. Tao, X.; Zhou, G.; Zhuang, X.; Cheng, B.; Li, X.; Li, H. Solution blowing of activated carbon nanofibers for phenol adsorption. *RSC Adv.* **2014**, *5*, 5801–5808. [CrossRef]
34. Diao, Z.-H.; Xu, X.-R.; Chen, H.; Jiang, D.; Yang, Y.-X.; Kong, L.-J.; Sun, Y.-X.; Hu, Y.-X.; Hao, Q.-W.; Liu, L. Simultaneous removal of Cr (VI) and phenol by persulfate activated with bentonite-supported nanoscale zero-valent iron: Reactivity and mechanism. *J. Hazard. Mater.* **2016**, *316*, 186–193. [CrossRef]
35. Lunagariya, J.; Chabhadiya, K.; Pathak, P.; Mashru, D. Application of Taguchi method in activated carbon adsorption process of phenol removal from ceramic gasifier wastewater. *Environ. Challenges* **2022**, *6*, 100450. [CrossRef]
36. Kamran, U.; Bhatti, H.N.; Iqbal, M.; Nazir, A. Green synthesis of metal nanoparticles and their applications in different fields: A review. *Z. Phys. Chem.* **2019**, *233*, 1325–1349. [CrossRef]
37. Giraldo, L.; Moreno-Piraján, J.C. Study of adsorption of phenol on activated carbons obtained from eggshells. *J. Anal. Appl. Pyrolysis* **2014**, *106*, 41–47. [CrossRef]
38. Sagbas, S.; Kantar, C.; Sahiner, N. Preparation of Poly(Humic Acid) Particles and Their Use in Toxic Organo-Phenolic Compound Removal from Aqueous Environments. *Water, Air, Soil Pollut.* **2013**, *225*, 1–10. [CrossRef]
39. Tamang, M.; Paul, K.K. Adsorptive treatment of phenol from aqueous solution using chitosan/calcined eggshell adsorbent: Optimization of preparation process using Taguchi statistical analysis. *J. Indian Chem. Soc.* **2022**, *99*, 100251. [CrossRef]
40. Issabayeva, G.; Hang, S.Y.; Wong, M.C.; Aroua, M.K. A review on the adsorption of phenols from wastewater onto diverse groups of adsorbents. *Rev. Chem. Eng.* **2017**, *34*, 855–873. [CrossRef]
41. Kazachenko, A.S.; Vasilieva, N.Y.; Fetisova, O.Y.; Sychev, V.V.; Elsuf'Ev, E.V.; Malyar, Y.N.; Issaoui, N.; Miroshnikova, A.V.; Borovkova, V.S.; Kazachenko, A.S.; et al. New reactions of betulin with sulfamic acid and ammonium sulfamate in the presence of solid catalysts. *Biomass Convers. Biorefinery* **2022**, 1–12. [CrossRef]
42. Fathy, M.; Selim, H.; Shahawy, A.E.L. Chitosan/MCM-48 nanocomposite as a potential adsorbent for removing phenol from aqueous solution. *RSC Adv.* **2020**, *10*, 23417–23430. [CrossRef]

43. Salari, M.; Dehghani, M.H.; Azari, A.; Motevalli, M.D.; Shabanloo, A.; Ali, I. High performance removal of phenol from aqueous solution by magnetic chitosan based on response surface methodology and genetic algorithm. *J. Mol. Liq.* **2019**, *285*, 146–157. [CrossRef]
44. Kamran, U.; Park, S.-J. Hybrid biochar supported transition metal doped MnO_2 composites: Efficient contenders for lithium adsorption and recovery from aqueous solutions. *Desalination* **2021**, *522*, 115387. [CrossRef]
45. Soni, U.; Bajpai, J.; Singh, S.K.; Bajpai, A. Evaluation of chitosan-carbon based biocomposite for efficient removal of phenols from aqueous solutions. *J. Water Process Eng.* **2017**, *16*, 56–63. [CrossRef]
46. Anirudhan, T.; Ramachandran, M. Removal of 2,4,6-trichlorophenol from water and petroleum refinery industry effluents by surfactant-modified bentonite. *J. Water Process Eng.* **2014**, *1*, 46–53. [CrossRef]
47. Hussain, A.; Dubey, S.K.; Kumar, V. Kinetic study for aerobic treatment of phenolic wastewater. *Water Resour. Ind.* **2015**, *11*, 81–90. [CrossRef]
48. Olu-Owolabi, B.I.; Alabi, A.H.; Diagboya, P.N.; Unuabonah, E.I.; Düring, R.-A. Adsorptive removal of 2,4,6-trichlorophenol in aqueous solution using calcined kaolinite-biomass composites. *J. Environ. Manag.* **2017**, *192*, 94–99. [CrossRef]
49. Loh, C.H.; Zhang, Y.; Goh, S.; Wang, R.; Fane, A.G. Composite hollow fiber membranes with different poly(dimethylsiloxane) intrusions into substrate for phenol removal via extractive membrane bioreactor. *J. Membr. Sci.* **2015**, *500*, 236–244. [CrossRef]
50. Sierra, J.D.M.; Wang, W.; Cerqueda-Garcia, D.; Oosterkamp, M.J.; Spanjers, H.; van Lier, J.B. Temperature susceptibility of a mesophilic anaerobic membrane bioreactor treating saline phenol-containing wastewater. *Chemosphere* **2018**, *213*, 92–102. [CrossRef]
51. Daramola, M.; Sadare, O.; Oluwasina, O.; Iyuke, S. Synthesis and Application of Functionalized Carbon Nanotube Infused Polymer Membrane (fCNT/PSF/PVA) for Treatment of Phenol-Containing Wastewater. *J. Membr. Sci. Res.* **2019**, *5*, 310–316. [CrossRef]
52. Ahmaruzzaman, M.; Gayatri, S.L. Activated Tea Waste as a Potential Low-Cost Adsorbent for the Removal of p-Nitrophenol from Wastewater. *J. Chem. Eng. Data* **2010**, *55*, 4614–4623. [CrossRef]
53. El-Naas, M.; Al-Zuhair, S.; Abu-Alhaija, M. Removal of phenol from petroleum refinery wastewater through adsorption on date-pit activated carbon. *Chem. Eng. J.* **2010**, *162*, 997–1005. [CrossRef]
54. Agarry, S.E.; Owabor, C.N.; Ajani, A.O. Modified plantain peel as cellulose-based low-cost adsorbent for the removal of 2,6-dichlorophenol from aqueous solution: Adsorption isotherms, kinetic modeling, and thermodynamic studies. *Chem. Eng. Commun.* **2013**, *200*, 1121–1147. [CrossRef]
55. Jabeen, A.; Bhatti, H.N.; Noreen, S.; Gaffar, A. Adsorptive removal of 2,4,6-trichloro-phenol from wastewater by mango seed shell and its magnetic composites: Batch and column study. *Int. J. Environ. Anal. Chem.* **2021**, 1–21. [CrossRef]
56. Hai, L.; Zhang, T.; Zhang, X.; Zhang, G.; Li, B.; Jiang, S.; Ma, X. Catalytic hydroxylation of phenol to dihydroxybenzene by Fe(II) complex in aqueous phase at ambient temperature. *Catal. Commun.* **2017**, *101*, 93–97. [CrossRef]
57. Kim, Y.-H.; Lee, B.; Choo, K.-H.; Choi, S.-J. Adsorption characteristics of phenolic and amino organic compounds on nano-structured silicas functionalized with phenyl groups. *Microporous Mesoporous Mater.* **2014**, *185*, 121–129. [CrossRef]
58. Kesavan, G.; Nataraj, N.; Chen, S.-M.; Lin, L.-H. Hydrothermal synthesis of $NiFe_2O_4$ nanoparticles as an efficient electrocatalyst for the electrochemical detection of bisphenol A. *New J. Chem.* **2020**, *44*, 7698–7707. [CrossRef]
59. Zhang, L.; Fang, P.; Yang, L.; Zhang, J.; Wang, X. Rapid Method for the Separation and Recovery of Endocrine-Disrupting Compound Bisphenol AP from Wastewater. *Langmuir* **2013**, *29*, 3968–3975. [CrossRef]
60. Freundlich, H.M.F. Über die adsorption in lösungen. *Z. Phys. Chem.* **1907**, *57U*, 385–470. [CrossRef]
61. Temkin, M.J.; Pyzhev, V. Recent modifications to Langmuir isotherms. *Acta Phys.Chim. Sin.* **1940**, *12*, 217–222.
62. Rahman, M.M.; Marwani, H.M.; Algethami, F.K.; Asiri, A.M.; Hameed, S.A.; Alhogbi, B. Ultra-sensitive p-nitrophenol sensing performances based on various Ag 2 O conjugated carbon material composites. *Environ. Nanotechnology, Monit. Manag.* **2017**, *8*, 73–82. [CrossRef]
63. Dubinin, M.M.; Raduskhevich, L.V. Proceedings of the academy of sciences of the USSR. *Phys. Chem.* **1947**, *55*, 327–329.
64. Hamdaoui, O.; Naffrechoux, E. Modeling of adsorption isotherms of phenol and chlorophenols onto granular activated carbon: Part I. Two-parameter models and equations allowing determination of thermodynamic parameters. *J. Hazard. Mater.* **2007**, *147*, 381–394. [CrossRef]
65. López-Luna, J.; Ramírez-Montes, L.E.; Martinez-Vargas, S.; Martínez, A.I.; Mijangos-Ricardez, O.F.; González-Chávez, M.D.C.A.; Carrillo-González, R.; Solís-Domínguez, F.A.; Cuevas-Díaz, M.D.C.; Vázquez-Hipólito, V. Linear and nonlinear kinetic and isotherm adsorption models for arsenic removal by manganese ferrite nanoparticles. *SN Appl. Sci.* **2019**, *1*, 1–19. [CrossRef]
66. Goel, J.; Kadirvelu, K.; Rajagopal, C.; Garg, V.K. Removal of lead(II) by adsorption using treated granular activated carbon: Batch and column studies. *J. Hazard. Mater.* **2005**, *125*, 211–220. [CrossRef]
67. Kamran, U.; Heo, Y.-J.; Min, B.-G.; In, I.; Park, S.-J. Effect of nickel ion doping in MnO_2/reduced graphene oxide nanocomposites for lithium adsorption and recovery from aqueous media. *RSC Adv.* **2020**, *10*, 9245–9257. [CrossRef]
68. Juang, R.-S.; Lin, S.-H.; Tsao, K.-H. Sorption of phenols from water in column systems using surfactant-modified montmorillonite. *J. Colloid Interface Sci.* **2003**, *269*, 46–52. [CrossRef]
69. Baek, K.W.; Song, S.H.; Kang, S.H.; Rhee, Y.W.; Lee, C.S.; Lee, B.J.; Hudson, S.; Hwang, T.S. Adsorption kinetics of boron by anion exchange resin in packed column bed. *J. Ind. Eng. Chem.* **2007**, *13*, 452–456.

70. Yousef, R.I.; El-Eswed, B. The effect of pH on the adsorption of phenol and chlorophenols onto natural zeolite. *Colloids Surfaces A: Physicochem. Eng. Asp.* **2009**, *334*, 92–99. [CrossRef]
71. Karunarathne, H.; Amarasinghe, B. Fixed Bed Adsorption Column Studies for the Removal of Aqueous Phenol from Activated Carbon Prepared from Sugarcane Bagasse. *Energy Procedia* **2013**, *34*, 83–90. [CrossRef]
72. Vijayaraghavan, K.; Jegan, J.; Palanivelu, K.; Velan, M. Removal of nickel(II) ions from aqueous solution using crab shell particles in a packed bed up-flow column. *J. Hazard. Mater.* **2004**, *113*, 223–230. [CrossRef] [PubMed]
73. Thomas, H.C. Heterogeneous Ion Exchange in a Flowing System. *J. Am. Chem. Soc.* **1944**, *66*, 1664–1666. [CrossRef]
74. Rao, K.; Anand, S.; Venkateswarlu, P. Modeling the kinetics of Cd(II) adsorption on Syzygium cumini L leaf powder in a fixed bed mini column. *J. Ind. Eng. Chem.* **2011**, *17*, 174–181. [CrossRef]
75. Oladipo, A.A.; Gazi, M. Fixed-bed column sorption of borate onto pomegranate seed powder-PVA beads: A response surface methodology approach. *Toxicol. Environ. Chem.* **2014**, *96*, 837–848. [CrossRef]
76. Cruz-Olivares, J.; Perez-Alonso, C.; Barrera-Díaz, C.; Ureña-Nuñez, F.; Chaparro-Mercado, M.; Bilyeu, B. Modeling of lead (II) biosorption by residue of allspice in a fixed-bed column. *Chem. Eng. J.* **2013**, *228*, 21–27. [CrossRef]
77. Jerold, M.; Vasantharaj, K.; Joseph, D.; Sivasubramanian, V. Fabrication of hybrid biosorbent nanoscale zero-valent iron-*Sargassum swartzii* biocomposite for the removal of crystal violet from aqueous solution. *Int. J. Phytoremediation* **2016**, *19*, 214–224. [CrossRef]
78. Kakavandi, B.; Jahangiri-Rad, M.; Rafiee, M.; Esfahani, A.R.; Babaei, A.A. Development of response surface methodology for optimization of phenol and p -chlorophenol adsorption on magnetic recoverable carbon. *Microporous Mesoporous Mater.* **2016**, *231*, 192–206. [CrossRef]
79. Motsa, M.M.; Thwala, J.M.; Msagati, T.A.M.; Mamba, B.B. Adsorption of 2,4,6-Trichlorophenol and ortho-Nitrophenol from Aqueous Media Using Surfactant-Modified Clinoptilolite–Polypropylene Hollow Fibre Composites. *Water, Air, Soil Pollut.* **2011**, *223*, 1555–1569. [CrossRef]
80. Pan, J.; Yao, H.; Li, X.; Wang, B.; Huo, P.; Xu, W.; Ou, H.; Yan, Y. Synthesis of chitosan/γ-Fe_2O_3/fly-ash-cenospheres composites for the fast removal of bisphenol A and 2,4,6-trichlorophenol from aqueous solutions. *J. Hazard. Mater.* **2011**, *190*, 276–284. [CrossRef]